Systematic Characterization of the Spectrum of Unilateral Finline

C. A. OLLEY AND T. E. ROZZI, SENIOR MEMBER, IEEE

Abstract—**The fundamental mode of finline is well documented. A sufficiently complete knowledge of the higher mode spectrum, however, is necessary for the treatment of discontinuities. This paper is concerned with a rigorous approach to the problem of the spectrum of unilateral finline on the basis of a variational solution in the space domain and transverse equivalent network considerations. We call this method transverse resonance diffraction. Having satisfied the correct edge condition *a priori*, the analysis produces highly accurate dispersion characteristics calculated at each "spot frequency" for the fundamental and higher order modes with matrices of very low order. By exploiting the quasi-analytical character of the model, it is possible to derive a systematic and complete characterization of the spectrum in terms of "mode families." Moreover, simple-to-use wide-band approximations to the dispersion characteristics are also obtained which are suitable for evaluation by a desktop calculator.**

I. INTRODUCTION

WITH THE INCREASED DEMAND for millimeter systems, *E*-plane structures such as finline have become established for use in millimeter-wave integrated circuits. Originally proposed by Meier [1], finline avoids unnecessary miniaturization at the millimeter frequencies while offering the potential for low-cost batch production and a degree of compatibility with active devices. Finline may be regarded as a form of planar ridged waveguide; this was recognized by Saad and Begemann [2], who produced approximate solutions for the fundamental mode using a simple equivalent circuit. Although the first fully rigorous solution was given earlier by Hofmann [3], this was time consuming and suffered from relative convergence problems. Saad and Schünemann [4] presented an analysis in terms of an equivalent set of rectangular waveguides to obtain a first-order design theory for simple finline filter sections, while Shih and Hoefer [5] applied the general TLM method with a view to obtaining the equivalent fin susceptance for a transverse resonance solution of the cutoff.

However, since 1979, the spectral-domain technique developed by Itoh and subsequently applied to finline [6] has been the accepted analysis. Subsequent papers [7], [8] have used this analysis to present results on the general properties of finline, including an assessment of loss, and have [9] extended the method to more general unilateral structures. Work has since been directed at the effect of finite fin thickness and substrate holding grooves using more general analyses, e.g., Beyer [10] and Wahldieck [11]. But, with certain exceptions [5], [6], most work has been directed at the fundamental mode. In addition, considerable computational effort is required even with the spectral-domain analysis, and this has led other authors to adopt approximate techniques, such as curve fitting (Pramanick and Bhartia [12]), and modified transverse resonance (Saad and Schünemann [13]). This motivates work towards rigorous approaches that yield simple and easy-to-use equivalent circuits.

Actual finline components, however, involve discontinuities. The solution of discontinuity problems, in turn, involves field matching with higher order modes. Therefore, in order for work to proceed on the analysis of finline discontinuities, such as in [15]–[16], a deeper understanding of the higher order modes is required. The identification of inductive and capacitive modes by Omar and Schünemann [17] is useful. Although LSE and LSM decoupling has been previously employed in the spectral-domain work, its significance was not fully appreciated.

We present an electromagnetic treatment which is rigorous but results in easy-to-use equivalent networks for the general solution and for cutoffs of various types of higher order mode. It also provides an accurate but simplified dispersion relation. The method operates in the space domain making use of transverse circuits and taking into explicit account the fins and their associated edge conditions. Restricting ourselves to the idealized unilateral finline structure as given by Fig. 1, the thickness of the fin metallization is ignored, as are any means of supporting the substrate. The transverse Green's admittances as seen at the fin aperture are obtained in the space domain; use is then made of the mapping, originally introduced by Schwinger [18], for the analysis of capacitive irises in waveguide, in order to introduce basis functions which implicitly satisfy the correct edge conditions. This judicious choice of basis yields rapid convergence with an exceptionally low order of required expansion.

With a view to characterizing the spectrum and obtaining simple but accurate broad-band equivalent circuits, we recognize two fundamental properties of hybrid modes in closed waveguide.

1) At cutoff, TE and TM contributions are decoupled, so that the Green's admittance becomes block diagonal and the resulting dispersion equation depends only on the

Manuscript received January 21, 1986; revised June 9, 1986. This work was supported in part by SERC under Grant 86352 and by Marconi Research.

The authors are with the School of Electrical Engineering, University of Bath, Claverton Down, Bath, England.

IEEE Log Number 8610284.

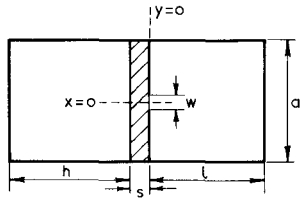

Fig. 1. Idealized unilateral finline.

cutoff wavenumber $k_0 = k_c$ rather than on k *and* the propagation constant β. This leads to a systematic and quasi-analytical determination of the cutoff wavenumbers k_c. A natural grouping of modes in "mode families" ensues, each family being characterized by a distinct quasi-static field in the gap.

2) Once the cutoff wavenumber of a mode is found, the propagation constant near cutoff must be expressible as an odd Laurent series of $\sqrt{k_0^2 - k_c^2}$ [19]. This realization leads naturally to an approximation for the dispersion equation, the simplest form of which is of the type

$$\beta = \eta\sqrt{k_0^2 - k_c^2}$$

with a real $\eta > 0$ virtually independent of frequency. This approximation we prefer to use over the "effective dielectric constant," which is still considerably frequency dependent.

II. Rigorous Analysis

The fields in finline will be described by y-directed Hertzian vector potentials coupled together in some way. Thus

$$\boldsymbol{E} = -j\omega\mu\nabla \times \Pi_h + k^2\Pi_e + \nabla\nabla\cdot\Pi_e \tag{1}$$

$$\boldsymbol{H} = k^2\Pi_h + \nabla\nabla\cdot\Pi_h + j\omega\epsilon\nabla \times \Pi_e \tag{2}$$

where

$$\Pi_h = \psi_h(x, y)e^{-j\beta z} \tag{3}$$

$$\Pi_e = \psi_e(x, y)e^{-j\beta z} \tag{4}$$

and propagation has been assumed in the z-direction with phase coefficient β.

For the analysis, the y-dependence of functions $\psi(x, y)$ is expressed in terms of the TE, TM (to y) eigenfunctions of slab-loaded waveguide $\chi_{hn}(y)$, $\chi_{en}(y)$. These are normalized so that $\chi_n(0) = 1$

$$\psi_h(x, y) = \sum_{n=0}^{\infty} U_{hn}\phi_{hn}(x)\chi_{hn}(y) \tag{5a}$$

$$\psi_e(x, y) = \sum_{n=1}^{\infty} U_{en}\phi_{en}(x)\chi_{en}(y) \tag{5b}$$

where

$$\phi_{hn}(x) = \sqrt{\frac{2}{a}}\cos\frac{n\pi}{a}x, \qquad n = 2,4,6,\cdots, \qquad -\frac{a}{2} \leqslant x \leqslant \frac{a}{2} \tag{6a}$$

$$= \sqrt{\frac{1}{a}}, \qquad n = 0$$

$$\phi_{en}(x) = \sqrt{\frac{2}{a}}\sin\frac{n\pi}{a}x. \tag{6b}$$

Moreover, at $y = 0$, it is possible to express four independent x and z field components in terms of the set $\{\phi_{hn}(x)\}$ only, by means of the choice below:

$$E_x(x,0) = \sum_{n=0}^{\infty} E_{xn}\phi_{hn}(x) \tag{7}$$

$$\frac{a}{\pi}\frac{\partial}{\partial x}E_z(x,0) = \sum_{n=1}^{\infty} E_{zn}\phi_{hn}(x) \tag{8}$$

$$\frac{\pi}{a}\int H_x(x,0)\,dx = \sum_{n=1}^{\infty} H_{xn}\phi_{hn}(x) \tag{9}$$

$$H_z(x,0) = \sum_{n=1}^{\infty} H_{zn}\phi_{hn}(x). \tag{10}$$

An additional advantage of using modified versions of E_z and H_x, namely, to produce proper convergence of the Green's functions, is discussed further in Appendix I.

The as yet unknown coefficients may be obtained from the modal amplitudes of transversely propagating pure TE and TM modes in the regions left and right of $y = 0$ using a now classical axis rotation due to Itoh [20]. The hybrid field is thus expressed in terms of voltages and currents upon TE and TM transmission lines. Eliminating voltages and currents leads to a direct relationship between the E and H fields. For instance, to the right of $y = 0$

$$\begin{bmatrix} -H_{zn} \\ H_{xn} \end{bmatrix} = \boldsymbol{N}\boldsymbol{T}_n^{-1}\begin{bmatrix} h_{nR} & 0 \\ 0 & g_{nR} \end{bmatrix}\boldsymbol{T}_n\boldsymbol{N}\begin{bmatrix} E_{xn} \\ E_{zn} \end{bmatrix} \tag{11}$$

where

$$\boldsymbol{T}_n = \begin{bmatrix} \cos\tau_n & -j\sin\tau_n \\ -j\sin\tau_n & \cos\tau_n \end{bmatrix}\boldsymbol{N}\begin{bmatrix} 1 & 0 \\ 0 & \dfrac{1}{n} \end{bmatrix}$$

$$\sin\tau_n = \frac{\beta}{\sqrt{\left[\dfrac{n\pi}{a}\right]^2 + \beta^2}}.$$

Here, h_{nR}, g_{nR} are the TM and TE admittances, respectively, seen by the nth mode looking right of $y = 0$, given by

$$h_{nR} = \frac{j\omega\epsilon}{k_{ny}}\coth k_{ny}l$$

$$g_{nR} = \frac{k_{ny}}{j\omega\mu}\coth k_{ny}l$$

where

$$k_{ny} = \sqrt{\left[\frac{n\pi}{a}\right]^2 + \beta^2 - k_0^2}.$$

From the above, by superposition, a relationship between the total fields left and right of the fin aperture may be formed. Thus, at $y = 0$ for the right-hand side of the

fin, we have in operator form,

$$\begin{bmatrix} -H_z \\ \frac{a}{\pi}\int H_x\,dx \end{bmatrix} = \begin{bmatrix} \tilde{Y}_{11}^R & \tilde{Y}_{12}^R \\ \tilde{Y}_{21}^R & \tilde{Y}_{22}^R \end{bmatrix} \cdot \begin{bmatrix} E_x \\ \frac{\pi}{a}\frac{\partial}{\partial x}E_z \end{bmatrix}. \quad (12)$$

It is noted that no distinction between fields right and left of the aperture need be made inasmuch as the fields are continuous there. On the left-hand side, we have

$$\begin{bmatrix} H_z \\ -\frac{a}{\pi}\int H_x\,dx \end{bmatrix} - \begin{bmatrix} \tilde{Y}_{11}^L & \tilde{Y}_{12}^L \\ \tilde{Y}_{21}^L & \tilde{Y}_{22}^L \end{bmatrix} \cdot \begin{bmatrix} E_x \\ \frac{\pi}{a}\frac{\partial}{\partial x}E_z \end{bmatrix}. \quad (13)$$

The sign difference on the left-hand sides of (12) and (13) is noted. This is a consequence of the opposite orientation of the Poynting vector at the two sides of the aperture.

The operator notation is defined as follows. For example,

$$-H_z|_{E_z=0} = \tilde{Y}_{11}^R \cdot E_x = \int_{-w/2}^{w/2} Y_{11}^R(x,x')E_x(x',0)\,dx'$$

where $Y_{11}^R(x,x')$, etc., are defined in Appendix I. It is noted here that $\tilde{Y}_{11}$ denotes the integral operator whose kernel is given by $Y_{11}(x,x')$. The matrix representation of Y_{11} in terms of a discrete basis will be indicated below by $\boldsymbol{Y}_{11}$, and elementwise by $(\boldsymbol{Y}_{11})mn$.

We now apply the continuity of fields at the fin aperture. By adding (12) and (13), one derives the following system of integral equations for E_x and $(\partial/\partial x)E_z$ involving the total cross-sectional admittance operators $\tilde{Y}_{11} = \tilde{Y}_{11}^R + \tilde{Y}_{11}^L$, etc:

$$\begin{bmatrix} \tilde{Y}_{11} & \tilde{Y}_{12} \\ \tilde{Y}_{21} & \tilde{Y}_{22} \end{bmatrix} \cdot \begin{bmatrix} E_x \\ \frac{a}{\pi}\frac{\partial}{\partial x}E_z \end{bmatrix} = 0 \quad (14)$$

where the corresponding Green's admittance functions are of the form

$$Y_{11}(x,x') = \sum_{n=0}^{\infty} Y_{11n}\phi_{hn}(x)\phi_{hn}(x')$$

$$Y_{12}(x,x') = \sum_{n=1}^{\infty} Y_{12n}\phi_{hn}(x)\phi_{hn}(x')$$

$$Y_{21}(x,x') = -Y_{12}(x,x')$$

$$Y_{22}(x,x') = \sum_{n=1}^{\infty} Y_{22n}\phi_{hn}(x)\phi_{hn}(x')$$

with Y_{11n}, etc., given in Appendix I.

In order to solve (14) by the Ritz–Galerkin method in real space, we expand the fields onto the orthonormal basis $\{f_m\}$ which satisfies the $r^{-1/2}$ singularity at the fin edges, as follows:

$$\begin{bmatrix} E_x(x) \\ \frac{a}{\pi}\frac{\partial}{\partial x}E_z(x) \end{bmatrix} \frac{dx}{d\theta} = \sum_{m=0}^{N} \begin{bmatrix} X_m \\ Z_m \end{bmatrix} f_m(\theta). \quad (15)$$

A suitable choice for the functions f_m is that originally introduced by Schwinger for the analysis of capacitive irises in waveguide [18] (see Appendix II).

The Schwinger functions result from the conformal mapping of the static fields between a parallel-plane waveguide and a waveguide with fin. Neglecting the slight perturbing effect of the dielectric, the quasi-static behavior of the fields in the fin gap is described exactly in terms of the above functions. The functions thus lend themselves as an ideal basis for use in a variational solution for finline. The perturbations due to the presence of the dielectric substrate and the proximity of the end walls, however, do not allow an exact solution directly from the mapping.

In the fin gap, we can also expand each ϕ_{hn} in terms of f_m, i.e.,

$$\phi_{hn} = \sum_{m=0}^{N} P_{mn} f_m. \quad (16)$$

The coefficients P_{mn} are defined in Appendix II. By application of (15) and (16) in (14), the latter is therefore transformed into a matrix equation

$$\begin{bmatrix} \boldsymbol{Y}_{11} & \boldsymbol{Y}_{12} \\ \boldsymbol{Y}_{21} & \boldsymbol{Y}_{22} \end{bmatrix} \begin{bmatrix} \boldsymbol{X} \\ \boldsymbol{Z} \end{bmatrix} = 0 \quad (17)$$

where

$$(\boldsymbol{Y}_{11})_{mk} = \sum_{n=0}^{\infty} y_{11n} P_{mn} P_{kn}$$

$$(\boldsymbol{Y}_{12})_{mk} = \sum_{n=1}^{\infty} y_{12n} P_{mn} P_{kn}$$

$$(\boldsymbol{Y}_{21})_{mk} = -(\boldsymbol{Y}_{12})_{mk}$$

$$(\boldsymbol{Y}_{22})_{mk} = \sum_{n=1}^{\infty} y_{22n} P_{mn} P_{kn}.$$

III. Transverse Equivalent Circuit in the Fundamental Finline Mode

The term $n=0$ in $\boldsymbol{Y}_{11}$ is the contribution of the fundamental "box" mode transverse to y (fundamental transverse mode). This is not yet the fundamental finline mode. By making this contribution explicit, however, it is possible to develop a convenient transverse equivalent circuit in the fundamental finline mode itself.

H_{z0} is the transverse magnetic field of the fundamental transverse mode (as $H_{x0}=0$). Due to the presence of the iris at $y=0$, the above is discontinuous by an amount $H_{z0}^L - H_{z0}^R = \Delta H_{z0}$. Let us extract the term $n=0$ from the summation in $\boldsymbol{Y}_{11}$ and write in place of the integral equation (17) an equivalent integral equation of the form

$$\Delta H_{z0}\begin{bmatrix} \boldsymbol{P}_0 \\ 0 \end{bmatrix} + \boldsymbol{Y}\cdot\begin{bmatrix} \boldsymbol{X} \\ \boldsymbol{Z} \end{bmatrix} = 0 \quad (18)$$

where $\boldsymbol{P}$ denotes the column vector P_m and

$$\boldsymbol{Y} = \begin{bmatrix} \sum_{n=1}^{\infty} y_{11n}\boldsymbol{P}_n\boldsymbol{P}_n^T & \boldsymbol{Y}_{12} \\ \boldsymbol{Y}_{21} & \boldsymbol{Y}_{22} \end{bmatrix}.$$

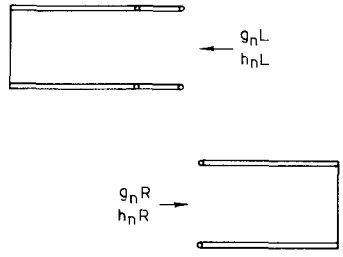

Fig. 2. Transverse admittances as seen by the fin

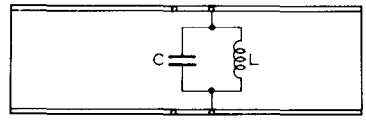

Fig. 3. Simplified equivalent circuit for the fundamental transverse mode.

TABLE I
COMPARISON OF ZEROTH-, FIRST-, SECOND-, AND THIRD-ORDER SOLUTIONS

Frequency/Ghz	Beta/ko			
	(0)	(1)	(2)	(3)
8.0	0.850961	0.849011	0.849001	0.849001
8.2	0.861708	0.859725	0.859716	0.859716
8.4	0.871585	0.869568	0.869558	0.869560
8.6	0.880684	0.878635	0.878627	0.878627
8.8	0.889091	0.887007	0.887000	0.887000
9.0	0.896874	0.894764	0.894754	0.894753
9.2	0.904111	0.901961	0.901936	0.901937
9.4	0.910834	0.908655	0.908678	0.908625
9.6	0.917112	0.914893	0.914884	0.914877
9.8	0.922993	0.920718	0.920709	0.920709
10.0	0.928497	0.926166	0.926158	0.926158
10.2	0.933679	0.931271	0.931263	0.931263
10.4	0.938332	0.936062	0.936055	0.936055
10.6	0.942864	0.940565	0.940559	0.940558
10.8	0.947132	0.944805	0.944798	0.944798
11.0	0.951156	0.948801	0.948794	0.948794
11.2	0.954954	0.952571	0.952564	0.952563
11.4	0.958546	0.956133	0.956126	0.956126
11.6	0.961945	0.959502	0.959495	0.959494
11.8	0.965167	0.962692	0.962684	0.962683
12.0	0.968224	0.965711	0.965703	0.965702

Solving for $\boldsymbol{X}$ gives

$$\boldsymbol{X} = -\Delta H_{z0}\left[\boldsymbol{Y}_{11} - \boldsymbol{Y}_{12}\boldsymbol{Y}_{22}^{-1}\boldsymbol{Y}_{21}\right]^{-1}\cdot\boldsymbol{P}_0. \tag{19}$$

The amplitude E_{x0} of the transverse field of the fundamental transverse mode (its voltage at $y=0$ in the equivalent circuit of Fig. 3) is given by

$$\boldsymbol{P}_0^T\cdot\boldsymbol{X} = E_{x0}.$$

This is related to the discontinuity in the transverse magnetic field (the current) by the total admittance seen by the mode at $y=0$, i.e.,

$$\Delta H_{z0} = (g_{0L} + g_{0R})E_{x0}$$

where g_{0L} and g_{0R} are the admittances seen by the fundamental transverse mode on either side of the fin (see Fig. 2). The fin itself is seen by the fundamental transverse mode as a transverse discontinuity whose admittance is given by

$$g = \left(\boldsymbol{P}_0^T\cdot\left[\boldsymbol{Y}_{11} - \boldsymbol{Y}_{12}\boldsymbol{Y}_{22}^{-1}\boldsymbol{Y}_{21}\right]^{-1}\cdot\boldsymbol{P}_0\right)^{-1}. \tag{20}$$

The condition of transverse resonance at $y=0$ gives therefore

$$g_{0L}(\beta, k_0) + g_{0R}(\beta, k_0) + g(\beta, k_0) = 0.$$

A solution for β at a given frequency k_0 is thus obtained at the resonance of the network given in Fig. 3. When solving for the fundamental mode, the higher order transverse modes are cutoff and therefore essentially localized about the fin. Thus, they can be represented as a fin admittance in terms of lumped components.

The order of matrix employed in the expression for the fin admittance g is determined by the size of expansion. But in view of the nature of the expansion set, the matrix order need not be increased beyond 2×2. In fact, the zeroth order is sufficient for all but very large fin gaps; furthermore, the term $\boldsymbol{Y}_{12}\cdot(\boldsymbol{Y}_{22})^{-1}\cdot\boldsymbol{Y}_{21}$ arising from E_x to E_z coupling may be ignored for small gaps and thin irises at least. Hence, by virtue of the Schwinger mapping,

$$g = y_{11}^s \ln\left|\csc^2\left[\frac{\pi w}{2a}\right]\right| + \sum_{n=1}^{nd}\left[y_{11n} - \frac{y_{11}^s}{n}\right]\frac{P_{n0}^2}{P_{00}^2}$$

where y_{11}^s/n is the limit of y_{11n} for large n, i.e., as $n\to\infty$, $y_{11n}\to y_{11}^s/n$. Its value is obtained by taking the above limit in Appendix I, which yields

$$y_{11}^s = \frac{2\beta^2 - (1+\epsilon_r)k_0^2}{\sqrt{\epsilon_r k_0^2 - \beta^2}\left[\frac{\pi}{a}\right]}.$$

It can be shown that the correction series converges rapidly and can be truncated after a few terms ($n > nd$).

For very small fin gaps, the correction series is negligible and in terms of the "effective frequency" variable

$$u = \sqrt{\epsilon_r k_0^2 - \beta^2}\left[\frac{a}{\pi}\right]$$

we can write

$$g = \frac{1}{juL} + juC$$

where

$$\frac{1}{L} = (\epsilon_r - 1)\left[\frac{a}{\pi}\right]^2 k_0^2 \ln\left|\csc^2\left[\frac{\pi w}{2a}\right]\right|$$

$$C = 2\ln\left|\csc^2\left[\frac{\pi w}{2a}\right]\right|$$

(see Fig. 3). Table I illustrates the convergence of the propagation constant of the fundamental finline mode for increasing order of the expansion for a moderately large fin gap ($w/a = 0.2$). The first column ($N=0$) corresponds to the above analytical formula including the correction series with $nd = 12$.

IV. CUTOFF PROPERTIES

It is apparent from (11) that at cutoff ($k = k_c$, $\beta = 0$) the off-diagonal blocks of the 2×2 Green's function vanish completely, so that the TE and TM components of the hybrid mode are decoupled. Also, at that point, only the cutoff wavenumber k_c enters the dispersion equation. The cutoff is, therefore, more easily determined as well as analytically approximated than the general case. Once the cutoff is found, it is also possible to identify specific

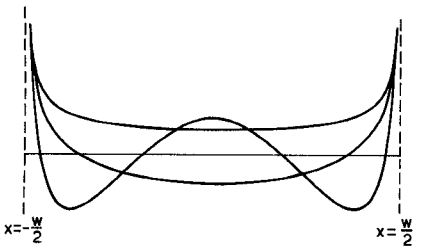

Fig. 4. Basis functions for LSE modes.

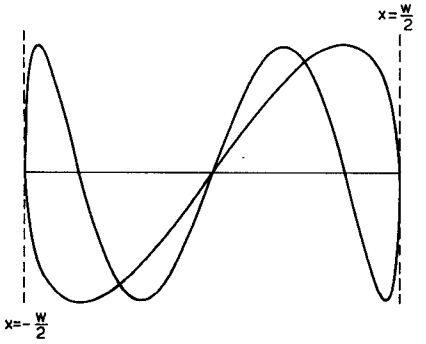

Fig. 5. Basis functions for LSM modes.

families of finline modes, and their individual $\beta - k$ characteristics not too far from cutoff can be approximated by means of a simple square root behavior. For these reasons, we will now consider the problem of determining cutoff in some detail.

As noted, at cutoff, the coupling matrices $\boldsymbol{Y}_{12}$ and $\boldsymbol{Y}_{21}$ vanish, and (17) reduces to

$$\boldsymbol{Y}_{11}\boldsymbol{X} = 0 \tag{21a}$$

$$\boldsymbol{Y}_{22}\boldsymbol{Z} = 0. \tag{21b}$$

Modes which are TE to y, i.e., LSE at cutoff, are obtained by setting $E_z = 0$ (i.e., $\boldsymbol{Z} = 0$).

Now orthogonal solutions of the quasi-static problem in the fin gap are given by

$$f_m(\theta) = \sqrt{\frac{2}{\pi}} \cos m\theta, \qquad m > 0$$

$$f_0(\theta) = \frac{1}{\sqrt{\pi}}.$$

The relationship between x and θ is established in (A3). The f_m's are in fact solutions to the quasi-static problem of the infinite parallel-plate waveguide with fin. In the x domain, these yield fin-gap fields, as shown in Figs. 4 and 5. Under quasi-static conditions, no coupling takes place between these solutions. Each value of m distinguishes therefore a whole family of modes (LSE(m) or LSM(m)) with the same quasi-static field in the gap at cutoff. Each member of the family, however, is a distinct solution of the dispersion equation arising from assuming that field distribution. Mathematically, this is expressed by the matrix $\boldsymbol{Y}_{11}$ becoming diagonal. Therefore, the transverse resonance condition (21a) reduces to each diagonal element being

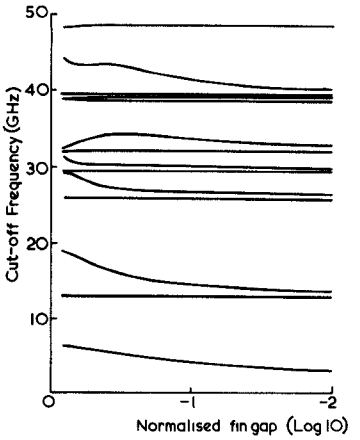

Fig. 6. Cutoff frequency versus fin gap for LSE(0) modes. Guide dimensions: $a = 10.16$ mm, $l = h + s = 11.43$ mm, $s = 0.254$ mm, $\epsilon_r = 2.20$.

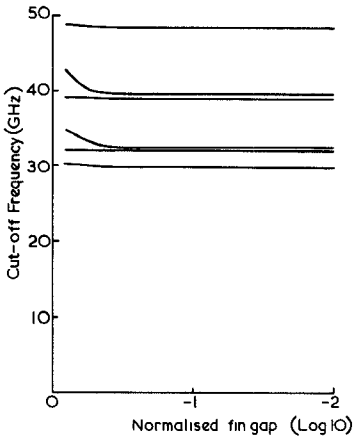

Fig. 7. Cutoff frequency versus fin gap of LSE(1) modes, dimensions as in Fig. 6.

individually zero, i.e.,

$$(\boldsymbol{Y}_{11})_{mm} = 0$$

or

$$\sum_{n=m}^{\infty} y_{11n}(k_{cm}) P_{mn}^2 = 0 \tag{22}$$

(since $P_{mn} = 0$ for $n < m$), which gives a very good approximation to the cutoff of the LSE(m) mode family.

For a given m, each solution of (22) (an infinite discrete set) corresponds to a member of the LSE(m) family. Similarly, the LSM(m) mode cutoffs are obtained from

$$\sum_{n=m}^{\infty} y_{22n}(k_{cm}) P_{mn}^2 = 0. \tag{23}$$

Note, in particular, that $m = 0$ variations for the LSM case are not acceptable since, from the definition of field quantities, this would represent a dc field in the fin gap.

From the solutions to (22) and (23), it is found that the fundamental finline mode is given by the first member of the LSE(0) family, corresponding to $m = 0$ field variation in the slot. This mode is therefore pure LSE at the cutoff point, although in general it is a hybrid HE mode.

Figs. 6 and 7 show the variation of cutoff frequencies versus the fin gap for the LSE(0) and LSE(1) mode fami-

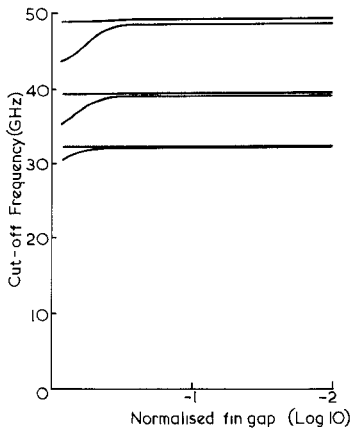

Fig. 8. Cutoff frequency versus fin gap of LSM(1) modes, dimensions as in Fig. 6.

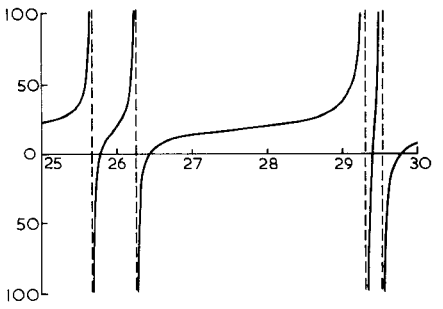

Fig. 9. Typical occurrence of roots to the cutoff equation, dimensions as in Fig. 6.

TABLE II
POSITION OF POLES OCCURRING IN SOLUTION FOR CUTOFF

LSE(0)	LSE(1)	LSM(1)
12.8375	-	-
13.1234	-	-
25.6719	-	-
26.2467	-	-
29.3099	29 3099	-
29.5275	29 5275	-
31.8687	31.8687	32.1964
32.3125	32.3125	32 3125
38.5000	-	-
38.8595	38.8595	39 1233
39.3701	-	-
39.5065	39 5065	39 5065
48.3023	48.3023	48 5125
49.2126	49 2126	49 2126

lies occurring below 50 GHz in an X-band finline. Notice that modes which display maximum E_x at $y = 0$ experience a pronounced reduction in cutoff as the fins intrude into the guide. This is due to their increased interaction. Those with a node at $y = 0$, however, starting with the first higher order finline mode, remain essentially unaffected by the fins. This is particularly so in the case of the highly symmetrical guide chosen in the analysis, where the central node of E_x occurs very near the plane of the fins.

Fig. 8 gives cutoffs for the first family of inductive modes, the LSM(1). As reported by Omar and Schünemann [17], the inductive modes experience an increase in cutoff as the fin gap is reduced. Although these changes should more appropriately be regarded as shifts away from modes of dielectrically loaded waveguide as the fin modes become established.

From Figs. 6–8, we therefore conclude that finline is LSE dominated (HE dominant in general). The first LSM-type mode typically occurs as the tenth higher order mode; however, the exact position in the mode spectrum depends upon the fin gap, since LSE and LSM cutoffs can cross over, leading to degeneracy when they coincide.

V. Asymptotic Behavior of Cutoff

We shall now examine (22) and (23) in some detail to discover any asymptotic behavior in the cutoff values which might be of use in any further work.

Now the elements y_{11n}, y_{22n} appearing in (22) and (23) correspond to field variations with x of order n. As the frequency is increased, a point is reached at which the corresponding parallel-plate mode becomes propagating and the modal admittances seen at either side of the fin begin to introduce tangent-type variations into the overall susceptance functions ((22) and (23)). The behavior of these functions therefore becomes progressively more complicated with cutoff frequency. However, the cutoffs given by zeros are straddled by poles of the admittance at either side of the fin. Thus, locating these poles leads to systematic solution for cutoffs by computer. Furthermore, poles and zeros increasingly cluster together, so that when searching for very high cutoffs (>100 GHz in the present case) it is sufficient to locate just the poles. Even for low cutoff values, the same effect of clustering is observed for very small fin gaps, as a consequence of a very large number of transverse modes being coupled to the fin-gap field.

Fig. 9 illustrates the occurrence of pole–zero pairs in the LSE(0) solution. Since the pole positions can be easily determined, the asymptotic cutoff frequencies can be obtained in a straightforward manner. Accurate solutions to (22) and (23) are only needed to provide a small number of corrections appropriate to the particular fin gap. Table II gives a list of poles relevant for the LSE(0), LSE(1), and LSM(1) solutions, confirming the above observations.

VI. Simplified Dispersion Equations

To complete the characterization of the finline modes, we return to the problem of describing their dispersion relationships by a simple expression of the form

$$\beta = \eta\sqrt{k_0^2 - k_c^2} \tag{24}$$

where k_c is the cutoff wavenumber previously obtained and η is now to be determined.

It has been shown that in a lossless, reciprocal, uniform waveguide, the propagation constant as a function of frequency can be expanded near cutoff as an odd Laurent series of $\sqrt{k_0^2 - k_c^2}$ [19]. In its simplest form, this expansion is just (24) where η is a constant.

As we now assume that η is a constant quantity, we therefore find the limit $k_0^2 \to 0$ of interest. At this point, the problem becomes quasi-static and since all the finline modes are cutoff in this limit, η can be determined from

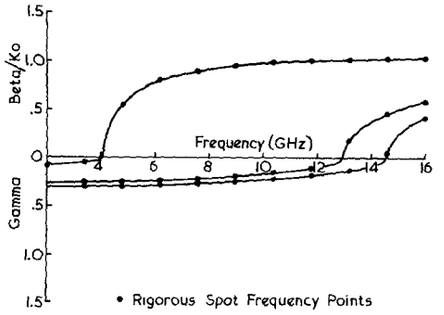

Fig. 10. Approximate dispersion curves with exact points for the first three modes, dimensions as in Fig. 6.

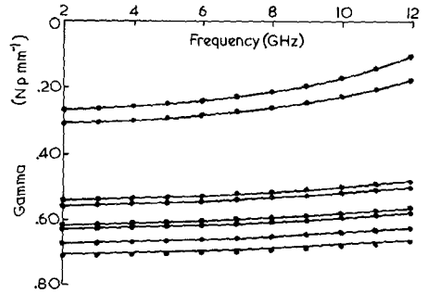

Fig. 11. Approximate dispersion of the following first eight higher order modes (with exact points), dimensions as in Fig. 6.

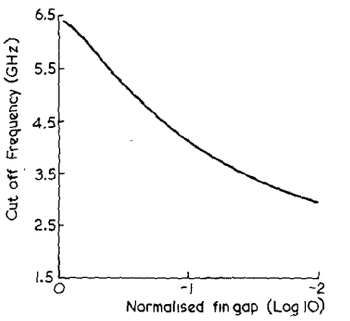

Fig. 12. Cutoff frequency for the fundamental mode in X-band finline, dimensions as in Fig. 6.

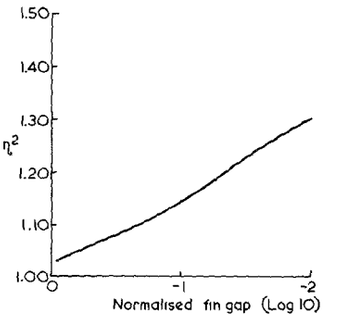

Fig. 13. η for the fundamental mode in X-band finline, dimensions as in Fig. 6.

the decay coefficient γ_0 and the cutoff wavenumber k_c

$$\eta = \frac{\gamma_0}{k_c}.$$

Before solving for γ_0, closer examination of the Green's admittance yields some useful simplifications, which greatly ease correlating the γ_0 with its respective k_c. As $k_0^2 \to 0$ we observe that all TM admittances vanish; furthermore, the air and substrate regions become indistinguishable to the TE modes. Thus, the effect of the dielectric is not felt and the problem becomes that of the static case in a finned waveguide. If, moreover, the fins are centrally placed in the finline enclosure, then it is noted that the coupling matrices Y_{12} and Y_{21} vanish, so that the solution for γ_0 of the LSE(m) and LSM(m) mode families decouples and can proceed as before.

Thus, γ_0 for the LSE(m) modes is given by

$$\sum_{n=m}^{\infty} y_{11n}(\gamma_0) P_{mn}^2 = 0$$

and for the LSM(m) modes by

$$\sum_{n=m}^{\infty} y_{22n}(\gamma_0) P_{mn}^2 = 0.$$

The assumption of a centrally placed fin leads to discrepancies with the higher order modes. But since they tend to propagate much more in the air region of the enclosure, η is sufficiently close to unity not to warrant further evaluation. However, an exception arises in the case of the third mode, which, like the fundamental, has strong interaction with the fins, and assuming $\eta = 1.0$ may not be sufficiently accurate. The second mode, as mentioned earlier, vanishes at $y = 0$ and is little affected by the fin; hence, η is very close to unity in any case.

Dispersion curves calculated for the first three modes give excellent agreement with the "spot frequency" results obtained with the rigorous analysis of Section II, since for these the symmetry assumption has little effect. Results for the dispersion of modes of even higher order assuming $\eta = 1.0$ are similarly very good, as shown in Figs. 10 and 11.

Finally, Figs. 12 and 13 give k_c and η for the fundamental mode for any given fin gap on a particular substrate. Such results can be readily incorporated into a curve fit for design purposes.

VII. Experimental and Theoretical Comparison

In order to assess validity, measurements of guided wavelength were performed using X-band finline with an adjustable fin gap. The method of observing the frequency response of a resonant length of line was employed, and in order to maintain a high Q factor, the short-circuited line was excited by small loop probes. Table III gives results for the fundamental mode, along with a comparison of two sets of theoretical predictions, one obtained with the method of Section II, the other by the established spectral-domain analysis. In both, a two-term expansion in the fin gap was used. However, the additional calculations required in the spectral-domain technique imply that the present method has a clear computational advantage, par-

TABLE III
COMPARISON OF EXPERIMENTAL RESULTS AND SPECTRAL-DOMAIN METHOD WITH PRESENT THEORY FOR THE FUNDAMENTAL MODE

Frequency/GHz	Guided wavelength /mm		
	Measured	Theoretical	
		Present method	Spectral domain
4 920	300 00	299 82	330 26
5 020	200 00	207 59	216 91
5 200	150 00	148 15	151 41
5 390	120 00	119 51	121 18
5 610	100 00	100 29	101 26
5 857	85 70	86 44	87 05
6 141	75 00	75.54	75 94
6 447	66 66	67.11	67 38
6.772	60.00	60.38	60 57
7.113	54.54	54 90	55 03
7.472	50.00	50.29	50.38
7 843	46.15	46.40	46.47
8.223	42.85	43.08	43 13
8.612	40.00	40.22	40 25
9.010	37.50	37 70	37 70
9 414	35.29	35 49	35 49
9.825	33 33	33.52	33 52
10 241	31 58	31 75	31 75
10.663	30.00	30 16	30 16
11.091	28.57	28 72	28 70
11.516	27.27	27.42	27 41
11 946	26.08	26.24	26 22
12.388	25.00	25.14	25 14

TABLE IV
EXPERIMENTAL MEASUREMENT OF THE FIRST HIGHER ORDER MODE COMPARED WITH SIMPLIFIED DISPERSION THEORY

Frequency/GHz	Guided wavelength /mm	
	Measured	Calculated
14 5034	46 15	46 22
14 7190	42 85	43 10
14 9634	40 00	40 20

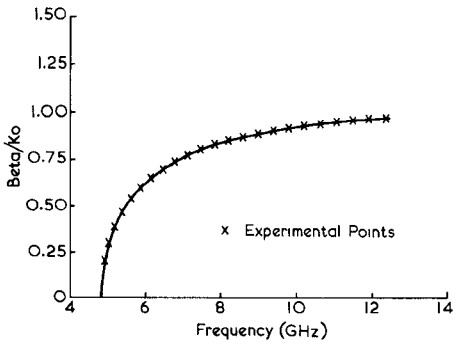

Fig. 14. Theoretical dispersion curve with experimental points, dimensions as in Fig. 6.

ticularly so when the accurate approximation of Section V is employed. Fig. 14 illustrates the excellent agreement between experimental and theoretical values. Finally, by operating the resonant line in the 14-GHz region, it was possible to discern resonances due to the first higher order mode. These compare very successfully with the theoretical predictions using $\eta = 1.0$ and $f_c = 12.97$ GHz in Table IV.

VIII. CONCLUSIONS

We have introduced a general and rigorous space-domain solution of unilateral finline based on transverse resonance diffraction. The affinity of the problem to that of a capacitive iris in waveguide is highlighted, and by satisfying *a priori* the appropriate edge condition, convergence is achieved with very low-order matrices. The quasi-analytic character of the treatment allows an accurate wide-band scalar dispersion equation for the fundamental mode as well as accurate approximate dispersion equations for the higher order modes to be derived. Finally, consideration of the cutoff properties of these modes results in a natural division of the spectrum in mode families and their characterization.

APPENDIX I

The admittances appearing in the sums under (14) are given by

$$y_{11n} = \cos^2\tau_n(h_{nR} + h_{nL}) + \sin^2\tau_n(g_{nR} + g_{nL})$$

$$y_{12n} = \frac{\cos\tau_n \sin\tau_n}{n}(h_{nL} - h_{nR} - g_{nL} + g_{nR})$$

$$y_{22n} = \frac{\cos^2\tau_n}{n^2}(g_{nR} + g_{nL}) + \frac{\sin^2\tau_n}{n^2}(h_{nR} + h_{nL}). \quad \text{(A1)}$$

It is now noted that the choice of (8) and (9) has the additional advantage of producing by integration by parts the factors n^{-1} in y_{12n} and n^{-2} in y_{22n} that ensure proper convergence. The exclusion of the $n = 0$ term from all but $y_{11}(x, x')$ arises naturally from the aforementioned definition of field quantities (1)–(10).

APPENDIX II

The Schwinger functions are derived from the conformal mapping between a parallel-plate waveguide and a system containing an iris. Such a mapping is of the general form

$$\cosh W = \alpha_1 + \alpha_2 \cosh T.$$

For the symmetrical case in question, the above mapping restricted to the x axis is

$$\cos\frac{2\pi x}{a} = \alpha_1 + \alpha_2\cos\theta \quad \text{(A2)}$$

such that

$$x = 0 \rightarrow \theta = 0$$

$$x = \frac{w}{2} \rightarrow \theta = \pi.$$

Thus

$$\alpha_1 = \cos^2\frac{\pi w}{2a} \quad \text{(A3a)}$$

$$\alpha_2 = \sin^2\frac{\pi w}{2a}. \quad \text{(A3b)}$$

We then find that the required singularity at $x = w/2$ is found in the term $\partial\theta/\partial x$ linking functions of θ to functions of x. Furthermore, the mapping now allows us to analytically determine certain infinite sums.

In the θ domain, we chose the basis set $\{f_m\}$, where

$$f_m(\theta) = \sqrt{\frac{2}{\pi}}\cos m\theta, \qquad m > 0$$

$$= \frac{1}{\sqrt{\pi}}, \qquad m = 0. \quad \text{(A4)}$$

This basis may be linked to the set (ϕ_{hn}) in the x domain

via the coefficients P_{mn}, such that

$$\phi_{hn}(x) = \sum_{m=0}^{n} P_{mn} f_m(\theta). \tag{A5}$$

It is clear from (6a), (A4), and (A2) that the first few coefficients are obtained as

$$P_{00} = \sqrt{\frac{\pi}{a}} \quad P_{01} = \sqrt{\frac{2\pi}{a}} \cos^2 \frac{\pi w}{2a}$$

$$P_{11} = \sqrt{\frac{\pi}{a}} \sin^2 \frac{\pi w}{2a}.$$

By considering Chebyshev polynomials, we can derive a recursive formula for generating further coefficients. Since

$$\cos \frac{2n\pi}{a} x = T_n\left[\cos \frac{2\pi}{a} x\right] = T_n(\alpha_1 + \alpha_2 \cos\theta) \tag{A6}$$

using the recursive formula

$$T_n(Z) = 2ZT_{n-1}(Z) - T_{n-2}(Z) \tag{A7}$$

with the trigonometric identity

$$\cos\theta \cos m\theta = \frac{1}{2}[\cos(m-1)\theta + \cos(m+1)\theta]$$

equation (A7) becomes

$$\begin{aligned}\sum_{m=0}^{n} P'_{mn} \cos p\theta &= 2\alpha_1 \sum_{m=0}^{n-1} P'_{m,n-1} \cos m\theta - \sum_{m=0}^{n-2} P'_{m,n-1} \cos m\theta \\ &\quad + \alpha_2 \sum_{m=-1}^{n-2} P'_{m+1,n-1} \cos m\theta \\ &\quad + \alpha_2 \sum_{m=1}^{n} P'_{m-1,n-1} \cos m\theta \end{aligned} \tag{A8}$$

where P'_{mn} are the coefficients linking the unnormalized sets

$$\left\{\cos \frac{2n\pi}{a} x\right\} \quad \text{and} \quad \{\cos m\theta\}.$$

Hence

$$\begin{aligned} P'_{mn} &= 2\alpha_1 P'_{m,n-1} - P'_{m,n-2} + \alpha_2 P'_{m+1,n-1} \\ &\quad + \alpha_2 \delta_{1,m} P'_{0,n-1} + \alpha_2 P'_{m-1,n-1} \end{aligned} \tag{A9}$$

$$\delta_{1,m} = \begin{cases} 0, & m \neq 1 \\ 1, & m = 1 \end{cases}$$

since, from (A2), (A3a), and (A3b), we have

$$P'_{00} = 1 \qquad P'_{01} + \cos^2 \frac{\pi w}{2a} \qquad P'_{11} = \sin^2 \frac{\pi w}{2a}$$

and the coefficients P'_{mn} can be generated as required. The coefficients P_{mn} are obtained directly from P'_{mn} by applying the normalization

$$P_{mn} = \sqrt{\frac{\delta_n}{\delta_m}} \sqrt{\frac{\pi}{a}} P'_{mn} \tag{A10}$$

where

$$\delta_n = 2, \quad n = 0$$
$$\delta_n = 1, \quad n > 0.$$

Acknowledgment

The authors wish to thank their colleagues C. Ryecroft, P. N. Sargeant, and S. F. Clarke of the Marconi Research Laboratories, Chelmsford, Essex, for many helpful discussions and their encouragement.

References

[1] P. J. Meier, "Integrated finline millimeter components," *IEEE Trans. Microwave Theory Tech.*, vol. MTT-22, pp. 1209–1216, Dec. 1974.

[2] A. M. K. Saad and G. Begemann, "Electrical performance of finlines of various configurations," *IEEE Trans. Microwaves, Opt., Acoust.*, vol. 1, pp. 81–88, Jan. 1977.

[3] H. Hofmann, "Finline dispersion," *Electron. Lett.*, vol. 12, no. 17, pp. 428–429, Aug. 1976.

[4] A. M. K. Saad and K. Schünemann, "A simple method for analyzing fin-line structures," *IEEE Trans. Microwave Theory Tech.*, vol. MTT-26, pp. 1002–1011, Dec. 1978.

[5] H.-C. Shih and W. Hoefer, "Dominant and second-order mode cutoff frequencies in fin lines calculated with a two-dimensional TLM program," *IEEE Trans. Microwave Theory Tech.*, vol. MTT-28, pp. 1443–1448, Dec. 1980.

[6] L.-P. Schmidt and T. Itoh, "Spectral domain analysis of dominant and higher order modes in fin-lines," *IEEE Trans. Microwave Theory Tech.*, vol. MTT-28, pp. 981–985, Sept. 1980.

[7] J. B. Knorr and P. M. Shayda, "Millimeter-wave fin-line characteristics," *IEEE Trans. Microwave Theory Tech.*, vol. MTT-28, pp. 737–743, July 1980.

[8] D. M-Syahkal and J. B. Davies, "An accurate, unified solution to various fin-line structures, of phase constant, characteristic impedance, and attenuation," *IEEE Trans. Microwave Theory Tech.*, vol. MTT-30, pp. 1854–1861, Nov. 1982.

[9] L. P. Schmidt, T. Itoh, and H. Hofmann, "Characteristics of unilateral fin-line structures with arbitrarily located slots," *IEEE Trans. Microwave Theory Tech.*, vol. MTT-29, pp. 352–355, Apr. 1981.

[10] A. Beyer, "Analysis of the characteristics of an earthed fin line," *IEEE Trans. Microwave Theory Tech.*, vol. MTT-29, pp. 676–680, July 1981.

[11] R. Vahldiek, "Accurate hybrid-mode analysis of various finline configurations including multilayered dielectrics, finite metallization thickness, and substrate holding grooves," *IEEE Trans. Microwave Theory Tech.*, vol. MTT-32, pp. 1454–1460, Nov. 1984.

[12] P. Pramanick and P. Bhartia, "Accurate analysis equations and synthesis technique for unilateral finlines," *IEEE Trans. Microwave Theory Tech.*, vol. MTT-33, pp. 24–29, Jan. 1985.

[13] A. M. K. Saad and K. Schünemann, "Closed-form approximations for fin-line eigenmodes," *Proc. Inst. Elec. Eng.*, pt. H. (MOA), vol. 129, pp. 253–261, Oct. 1982.

[14] R. Sorrentino and T. Itoh, "Transverse resonance analysis of finline discontinuities," *IEEE Trans. Microwave Theory Tech.*, vol. MTT-12, pp. 1633–1638, Dec. 1984.

[15] K. J. Webb and R. Mittra, "Solution of the finline step-discontinuity problem using the generalized variational technique," *IEEE Trans. Microwave Theory Tech.*, vol. MTT-33, pp. 1004–1100, Sept. 1985.

[16] A. S. Omar and K. Schünemann, "Transmission matrix representation of finline discontinuities," *IEEE Trans. Microwave Theory Tech.*, vol. MTT-33, pp. 765–770, Sept. 1985.

[17] ——, "Space domain decoupling of LSE and LSM fields in generalized planar guiding structures," *IEEE Trans. Microwave Theory Tech.*, vol. MTT-32, pp. 1626–1632, Dec. 1984.

[18] R. E. Collin, *Field Theory of Guided Waves*. New York: McGraw-Hill, 1960, ch. 8.

[19] J. D. Rhodes, "General constraints on propagation characteristics of electromagnetic waves in uniform inhomogeneous waveguides," *Proc. Inst. Elec. Eng.*, vol. 118, no. 7, pp. 849–856, 1971.

[20] T. Itoh, "Spectral domain immittance approach for dispersion characteristics of generalised printed transmission lines," *IEEE Trans. Microwave Theory Tech.*, vol. MTT-28, pp. 733–736, July 1980.

✠

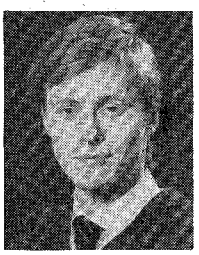

C. A. Olley was born in Bath, U.K., in 1960. He obtained the B.Sc. (with honors) degree in electrical engineering from Bath University in 1983. Since then, he has been working towards the Ph.D. degree in the area of finline characterization under the sponsorship of the Science and Engineering Research Council and of GEC-Marconi research at Great Baddow, Essex.

Mr. Olley is a Student Member of the Institution of Electrical Engineers (IEE) and of the Institution of Electronic and Radio Engineers (IERE), U.K. He was awarded the IEE Student Prize in 1981 and the IEE South Western Region Young Members Award in 1985.

✠

T. E. Rozzi (M'66–SM'74) obtained the degree of Dottore in physics from the University of Pisa in 1965 and the Ph.D. degree in electronic engineering from Leeds University in 1968.

From 1968 to 1978, he was a research scientist at the Philips Research Laboratories, Eindhoven, the Netherlands, having spent one year (1975) at the Antenna Laboratory, University of Illinois, Urbana. In 1978, he was appointed a Chair of Electrical Engineering at the University of Liverpool. In 1981, he was appointed the Chair of Electronics and was made Head of the Electronics Group at the University of Bath. From 1983 to 1986, he held the additional responsibility of Head of the School of Electrical Engineering at Bath. Since 1986, Prof. Rozzi has also held the "ordinary chair" of Antennas at the Faculty of Engineering, University of Ancona, Italy.

In 1975, Prof. Rozzi was awarded the Microwave Prize of the Microwave Theory and Technique Group of the Institute of Electrical and Electronic Engineers.